Nanoscience and Nanotechnology Letters
Vol. 9, 567–572, 2017

Formation Mechanism of Strontium Hexaferrite Compounds by Complementary Structure and Thermogravimetry Investigations

Li Xu[1,*], Haizhu Wang[1,2], Ying Xu[3], Quhui Wang[1], Xiaohui Ma[1], Zhe Zhou[4], Yonggang Zou[1], and Scott Xing[5]

[1] *State Key Laboratory of High Power Semiconductor Laser, Changchun University of Science and Technology, Changchun 130022, People's Republic of China*
[2] *State Key Joint Laboratory of Environment Simulation and Pollution Control (SKJLESPC), Beijing Key Laboratory for Emerging Organic Contaminants Control, School of Environment, POPs Research Center, Tsinghua University, Beijing, 100084, People's Republic of China*
[3] *School of Physics, Northeast Normal University, Changchun 130024, People's Republic of China*
[4] *Changchun Institute of Optics, Fine Mechanics and Physics, Chinese Academy of Sciences, Changchun 130033, People's Republic of China*
[5] *Specialty Technology Development Department, United Microeletronics Corporation, Singapore 519528, Singapore*

Strontium hexaferrite ($SrFe_{12}O_{19}$) compounds with hexagonal structure are fabricated by sintering the mixture of α-Fe_2O_3 and $SrCO_3$ and ball milling the mixture of α-Fe_2O_3 and $SrCO_3$ followed by heat treatment, respectively. The mechanism of formation of the $SrFe_{12}O_{19}$ in the two kinds of procedures was investigated by using both thermogravimetry and X-ray diffractometer measurements. It was found that the α-Fe_2O_3 reacted with $SrCO_3$ to form $SrFeO_{2.97}$ with cubic structure as the mixture was sintered above 750 °C firstly and then the $SrFeO_{2.97}$ reacted with α-Fe_2O_3 to form $SrFe_{12}O_{19}$ in a sintering temperature ranging from 750 to 960 °C. However, the α-Fe_2O_3 reacted with $SrCO_3$ to form Sr-containing Fe_3O_4 with spinel structure when the mixture was milled for 120 h, while the $SrFe_{12}O_{19}$ was obtained by annealing the Sr-containing Fe_3O_4 at 700–1000 °C. The magnetic properties of the $SrFe_{12}O_{19}$ produced by the two kinds of procedures were reached. The saturation magnetization and the coercivity of the $SrFe_{12}O_{19}$ fabricated by ball milling followed by heat treatment were 60.65 emu/g and 5481.1 G, respectively, which were much larger than those of the $SrFe_{12}O_{19}$ produced by the other procedure. The mechanism leading to that the $SrFe_{12}O_{19}$ produced by the different methods had different magnetic properties was discussed in the present work.

Keywords: Strontium Hexaferrite, Thermogravimetry Curve, Magnetic Properties.

1. INTRODUCTION

Hexagonal ferrites $MFe_{12}O_{19}$ (M = Ba, Sr, Pb), with a magnetoplumbite structure type are widely used for technological applications. In particular, strontium hexaferrites, due to the magnetic properties of strontium hexaferrite is much larger than other hexagonal ferrites, are used for their hard magnetic properties. It can also be found that there are a wide range of applications in magnetic recording media, electronic devices, medicine and magneto-optical recording.[1–6]

Doping engineering is widely used to tailor the band structures of bulk and nanoscale materials, promising and facilitating the construction of various multifunctional materials and devices.[7–26] To date, many studies in this field have focused on improving magnetic properties of strontium hexaferrite by variety of synthesis methods and doping elements. Such as: Zn–Sn substituted strontium hexaferrite is prepared by sol–gel method,[27] Nd and Co substituted strontium hexaferrite is prepared by self-combustion method,[28] Zr–Cd substituted is synthesized by the chemical co-precipitation technique,[6] and so on. However, these substitutions can cause the intrinsic coercivity to decrease effectively but at the expense of decrease in saturation magnetization. Therefore, the cationic substitutions are not a suitable way to alter magnetic properties of strontium hexaferrite. And then, the formation of

*Author to whom correspondence should be addressed.

strontium hexaferrite all undergoes the intermediate phase in the variety of synthesis processes. Whereas the intermediate phase transformation is often overlooked in the formation of strontium hexaferrite process. In fact, the different intermediate phase transformation will have a great impact on the magnetic properties of strontium hexaferrite during the formation of strontium hexaferrite.[29]

Mechanochemistry is concerned with chemical transformations induced by mechanical means, such as compression, shear, or friction. Unintentional chemical reactions accompany many forms of mechanical action, like grinding, sliding, or plastic deformation, while the deliberate application of mechanical energy, typically by means of high-energy ball milling, provides a method to prepare useful new materials and to improve the efficiency of complex processes.[30–33] However, the reports on preparing strontium hexaferrite using mechanochemical technology are not many. In fact, the different preparation methods and intermediate phase transformation will have a great impact on the magnetic properties of strontium hexaferrite during the formation of strontium hexaferrite.[29]

The conventional sinter method and the mechanical alloy method are two common methods of preparing strontium hexaferrite. In this work, the two methods are used to synthesize strontium hexaferrite. The purpose is to reveal that the intermediate phase transformations of two kinds of procedures are different in the formation of strontium hexaferrite process and the different phase transformation have a great influence on the magnetic properties of strontium hexaferrite in the aspects of equilibrium condition and non-equilibrium condition.

2. EXPERIMENTAL PROCEDURES

A mixture of 99% pure nonmagnetic α-Fe_2O_3 and $SrCO_3$ powders were used as starting materials for production of $SrFe_{12}O_{19}$ by conventional sinter method and mechanochemical reaction in a high-energy ball milling. The molar ratio of α-Fe_2O_3 to $SrCO_3$ was 3:1 in the mixture. In the conventional sinter process, the mixture was sintered from room temperature to 1000 °C. In the mechanochemical reaction process, the mixture was milled in a mill firstly and annealed under ordinary pressure ambient in a temperature ranging from room temperature to 1000 °C. A stainless vial filled with stainless balls having diameter of 5–15 mm was used as the milling medium. The mass of the mixture was 7 g and the balls-to-powder mass ratio was 15:1. The mixture was milled under air ambient without any additives (dry milling). These samples were pressed into disk (under pressure of 0.2 GPa) and sintered for 2 h in air atmosphere in a temperature ranging from 700 to 1000 °C.

The structure of the samples was characterized by using a Rigaku-D-Max X-ray diffractometer (XRD) with $Cu_{K\alpha}$ radiation ($\lambda = 1.5418$ Å). The thermal behaviors of the samples were examined by thermogravimetric and differential scanning calorimeter (TG/DTA, STA 449C, Netzsch) in a temperature ranging from room temperature to 1000 °C with a heating rate of 10 °C/min. Measurement of magnetic properties were performed in a vibrating sample magnetometer (VSM) at room temperature with a maximum applied field of 1100 kA/m. (Lake Shore 7410 vibrating sample magnetometer).

3. RESULTS AND DISCUSSION

Figure 1(a) shows the XRD patterns of the mixture of α-Fe_2O_3 and $SrCO_3$ powders with molar ratio of 3:1, indicating that the mixture consists of α-Fe_2O_3 and $SrCO_3$ with rhombohedra and orthorhombic structure, respectively. Using the mixture as starting material, we try to fabricate strontium hexaferrite ($SrFe_{12}O_{19}$) by conventional sinter method. In order to understand the mechanism of formation of the $SrFe_{12}O_{19}$, a TG curve for the mixture powders was measured in a temperature ranging from room temperature to 1000 °C, as shown in solid line in Figure 2(a). In order to better understand the sintering reaction process of the mixture by the TG curve, the curve is differentiated, and the differential result is also shown by dot line in Figure 2(a). As AB segment of the curve in Figure 2(a) shows, the mass of the mixture decreases slowly with increasing temperature between room temperature and 300 °C, while the mass of the mixture has no change in a temperature ranging from 300 to 750 °C, as shown in BC segment. The former is due to the release of gas and the vapor absorbed on the surface of the mixture, and the latter implies there is no chemical reaction between α-Fe_2O_3 and $SrCO_3$. However, when the temperature exceeds 750 °C, the TG curve begins to decrease nonlinearly till the temperature up to about 960 °C, as shown in CD segment of the curve, implying that a chemical reaction may occur. In order to demonstrate this reaction,

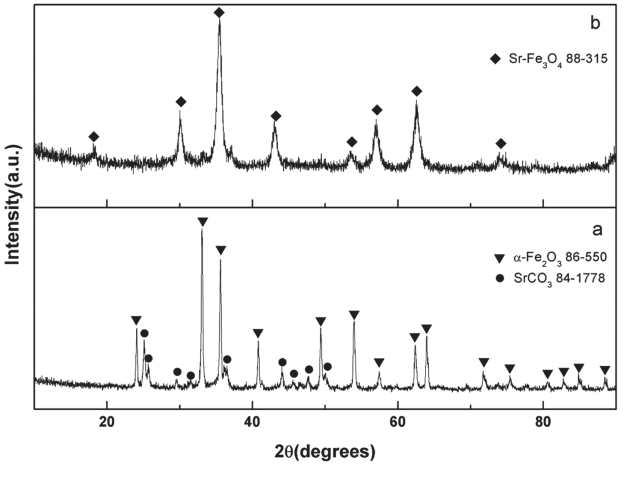

Fig. 1. XRD patterns for conventional sinter route (a) and 120 h ball-milled $SrCO_3$+$3Fe_2O_3$ (b) powders: (▼) α-Fe_2O_3; (●) $SrCO_3$; (♦) Sr-Fe_3O_4.

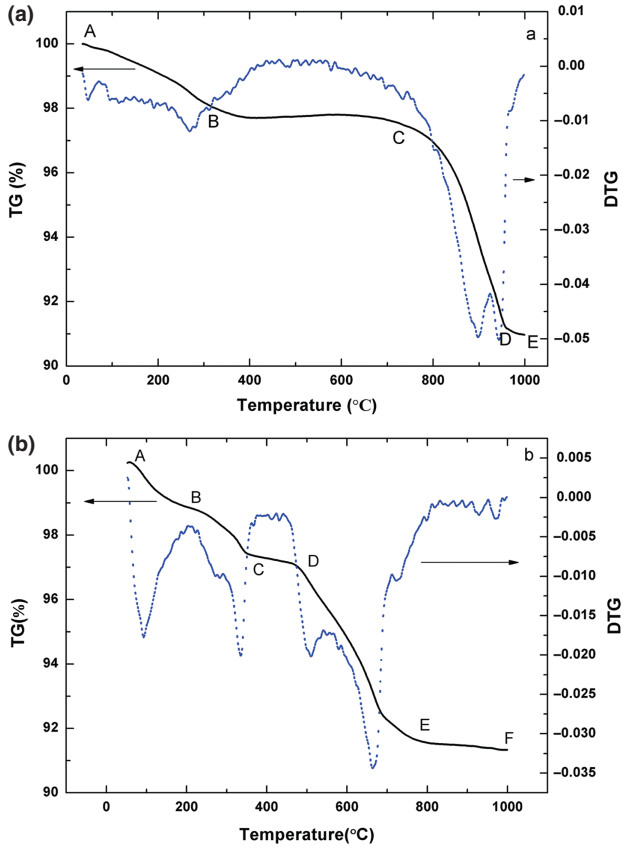

Fig. 2. TG curves of precursor powders which were prepared by conventional sinter route (a) and high energy ball milling in air: solid shows the TG curve; blue dot line shows differential line of TG curve samples.

the mixture is sintered for 2 h at 800 °C in air ambient. Figure 3(a) shows the XRD pattern of the sintered mixture. It is found that the intensity of diffraction peaks of $SrCO_3$ decreases greatly, meanwhile, some additional diffraction peaks are observed in the XRD profile besides the diffraction peaks of α-Fe_2O_3. These additional peaks are demonstrated to be the diffractions of $SrFeO_{2.97}$ with cubic structure. This implies that the α-Fe_2O_3 reacts with $SrCO_3$ to form $SrFeO_{2.97}$ with cubic structure as they are sintered at 800 °C in air ambient, accompanied by release of CO_2. The reaction can be expressed as follows:

$$SrCO_3 + \alpha - Fe_2O_3 \rightarrow SrFeO_{2.97} + CO_2 \uparrow$$

The dot line in Figure 2(a) indicates that variation rate of TG curve fraction with temperature changing in CDE segment, which implies that some additional chemical reaction may occur in the segment besides the reaction between α-Fe_2O_3 and $SrCO_3$. In order to understand the additional reaction, the mixture is sintered for 2 h at 1000 °C, and measured by XRD, as shown in Figure 4 (a). In comparison with the Figure 3(a), the intensity of diffraction peaks of the $SrFeO_{2.97}$ decreases greatly and the diffraction peaks of the α-Fe_2O_3 are not almost observed in Figure 4(a), meanwhile, the diffraction peaks of strontium hexaferrite are observed and become dominant, while the diffraction peaks of the α-Fe_2O_3 completely disappear. The results of Figures 3(a) and 4(a) indicate that the mixture sintered at 1000 °C mainly consists of $SrFe_{12}O_{19}$ and a small amount of $SrFeO_{2.97}$. The $SrFe_{12}O_{19}$ is formed by following reaction process:

$$SrFeO_{2.97} + \alpha\text{–}Fe_2O_3 \rightarrow SrFe_{12}O_{19}$$

Based on the above discussion, the formation of the $SrFe_{12}O_{19}$ can be deduced as follows: firstly, the α-Fe_2O_3 reacts with $SrCO_3$ to form $SrFeO_{2.97}$ when the sintering temperature is above 750 °C, and then the $SrFeO_{2.97}$ begins to react with α-Fe_2O_3 to form $SrFe_{12}O_{19}$ as the sintering temperature is higher than 900 °C, this reaction completes at about 960 °C. Since no reaction occurs above 960 °C,

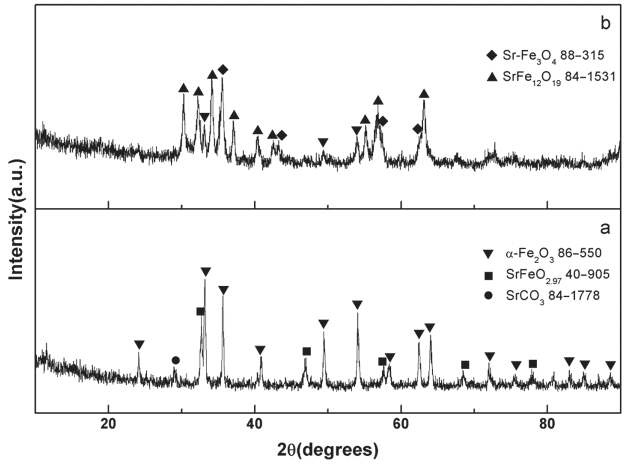

Fig. 3. The XRD diffraction patterns of precursor powders which were prepared by conventional sinter route sintered for 2 h at 800 °C (a) and ball milling sintered for 2 h at 700 °C (b): (▼) α-Fe_2O_3; (●) $SrCO_3$; (♦) Sr-Fe_3O_4; (■) $SrFeO_{2.97}$; (▲) $SrFe_{12}O_{19}$.

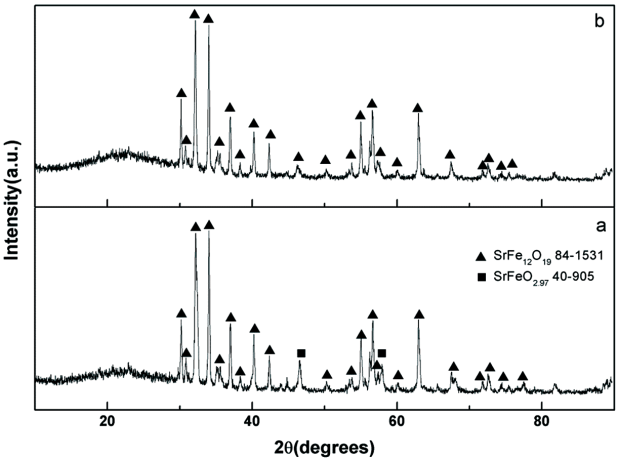

Fig. 4. The XRD diffraction patterns of $SrFe_{12}O_{19}$ prepared by conventional sinter route (a) and ball milling (b) for 2 h at 1000 °C: (■) $SrFeO_{2.97}$; (▲) $SrFe_{12}O_{19}$.

the TG curve fraction also does not change, as shown in DE segment in Figure 2(a).

The mixture of the $SrCO_3$ and α-Fe_2O_3 powders as the starting materials is milled for 120 h. Expressly after ball milling for 120 h, the mixture is completely different from the starting materials, the color of mixture changes slowly from red to black. Figure 1(b) shows the XRD diffraction pattern of the mixture milled for 120 h, indicating that the diffraction peaks of the $SrCO_3$ and α-Fe_2O_3 disappear completely, while some strong diffraction peaks belonging to the Sr-containing Fe_3O_4 with spinel structure are observed. That implies that some α-Fe_2O_3 react with $SrCO_3$ to form Sr-containing Fe_3O_4 with spinel structure. The 120 h-milled mixture consists of a single Sr-containing Fe_3O_4 phase.

Now we try to fabricate the strontium hexaferrite by sintering the 120 h-milled mixture. In order to understand the mechanism of formation of the $SrFe_{12}O_{19}$ in the sintering process, a TG curve for the 120 h-milled mixture is measured in a temperature ranging from room temperature to 1000 °C, as shown in solid line in Figure 2(b). In order to better understand the sintering reaction process of the 120 h-milled mixture by the TG curve, the curve is differentiated, and the differential result is also shown by dot line in Figure 2(b). Being different from the TG curve (a), the TG curve (b) keeps on decreasing in the whole temperature coverage. In the TG profiles, three weight losses in a temperature ranging from room temperature to 800 °C are observed in the TG curve. As ABC segment of the curve in Figure 2(b) shows, the TG curve of 120 h-milled sample decreases sharply with increasing temperature in a temperature ranging from room temperature to around 200 °C and then in the other temperature between 200 and 400 °C. The contraction in AB segment is due to the evaporation of adsorbed vapor, while the contraction in BC segment is attributed to the evaporation of absorbed gases. When the temperature exceeds 500 °C, the TG curve begins to decrease quickly till the temperature up to 800 °C, as shown in DE segment of the curve, implying that a chemical reaction may occur. In order to understand this reaction , the 120 h-milled sample is pressed into disk and sintered for 2 h at 700 °C in air ambient. Figure 3(b) shows the XRD diffraction patterns of the 120 h-milled sample sintered. It is found that the diffraction peaks of Sr-containing Fe_3O_4 phase with spinel structure almost disappear, while the diffraction peaks of α-Fe_2O_3 and $SrFe_{12}O_{19}$ phases are observed, comparing with $SrFe_{12}O_{19}$ prepared by conventional sinter method, where the synthesis temperature $SrFe_{12}O_{19}$ phases occurs at 960 °C, as shown in Figure 2(a).

The dot line in Figure 2(b) indicates that variation rate of the TG curve with temperature has obvious change in DE segment of the TG curve, which implies that a chemical reaction may occur in the segment. In order to further understand the chemical reaction, the 120 h-milled mixture is sintered for 2 h at 1000 °C in air ambient, its XRD pattern is shown in Figure 4(b). In comparison with the Figure 3(b), the intensity of diffraction peaks of $SrFe_{12}O_{19}$ increases greatly and the diffraction peaks of α-Fe_2O_3 and Sr-containing Fe_3O_4 disappear completely, no diffraction peaks of other phase can be observed. We suppose that the chemical reaction can be expressed as follow:

$$2Sr + 8Fe_3O_4 + 3O_2 \uparrow \rightarrow 2SrFe_{12}O_{19}$$

The release of the O_2 leads to decrease in weight, in agreement with the TG curve of weight loss in Figure 2(b). Based on the above discussion, the formation of $SrFe_{12}O_{19}$ can be deduced as follows: Firstly, the Sr-containing Fe_3O_4 is fabricated by mechanochemical reaction of α-Fe_2O_3 and $SrCO_3$, and then the Sr-containing Fe_3O_4 transforms into $SrFe_{12}O_{19}$ phase when it is sintered at the temperatures of 500–800 °C. With increasing temperature, the content of α-Fe_2O_3 decreases gradually, the content of the $SrFe_{12}O_{19}$ turns to be much more and more compact so that the sintering curve decreases from the beginning of 800 up to 1000 °C, so the TG fraction continues to slightly decrease, as shown in EF segment in Figure 2(b).

The hysteresis loops of two selected samples which are fabricated by sintering the mixture of α-Fe_2O_3 and $BaCO_3$ (loop A) and the 120 h-milled mixture (loop B) for 2 h at 1000 °C, are shown in Figure 5. From the VSM experiments, the magnetic parameters such as saturation magnetization (M_S), coercivity (H_C) and remnant magnetization (M_r) are given in Table I.

From the Table I, it is clearly seen that two experiment samples have similar value of saturation magnetization and remnant magnetization of $SrFe_{12}O_{19}$ which was fabricated by sintering 120 h-milled mixture and conventional sinter method, respectively. However, the coercivity of $SrFe_{12}O_{19}$ fabricated by sintering 120 h-milled mixture is much larger than the other $SrFe_{12}O_{19}$ sample produced by conventional sinter method. Moreover, the coercivity

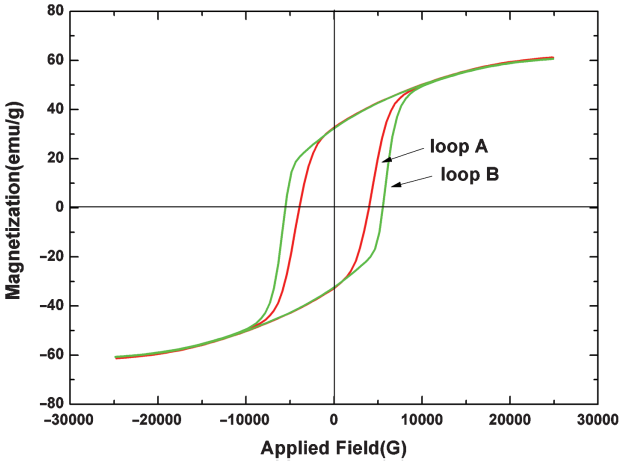

Fig. 5. Hysteresis loops of the precursor powders which were prepared by conventional sinter route (a) (loop A: red curve) and ball milling (b) (loop B: green curve) for 2 h at 1000 °C.

Table I. Magnetic properties of $SrFe_{12}O_{19}$ by sintering two starting materials.

	Saturation magnetization (emug)	Remnant magnetization (emug)	Coercivity (G)
Hysteresis loop A	61.14	32.60	3932.4
Hysteresis loop B	60.65	32.32	5481.1

of $SrFe_{12}O_{19}$ fabricated by sintering 120 h-milled mixture is better than the coercivity of $SrFe_{12}O_{19}$ in the literature reported previously.[1] Generally, the coercivity of $SrFe_{12}O_{19}$ is related to purity, grain size, pinning and so on. The apparent grain size of samples is estimated by analyzing the X-ray diffraction peak broadening, using Scherrer's equation: $\langle D\rangle = 0.89\lambda/\beta_{1/2}\cos\theta$, here $\langle D\rangle$ is the average particle size, λ is the wavelength of the incident X-ray, θ is the corresponding Bragg angle and $\beta_{1/2}$ is the full-width at half-maximum (FWHM) of the XRD peak. The result shows that the grain sizes of $SrFe_{12}O_{19}$ prepared by the two kinds of techniques are similar to each other, 30.01 nm (Fig. 4(a)) and 30.91 nm (Fig. 4(b)) respectively, which indicating that the grain size is not the major influencing factor of the different coercivity of strontium hexaferrite. As can be seen from Figure 4, according to the comparison with the $SrFe_{12}O_{19}$ of ICCD card No. 84-1531 and the change of relative intensity and position of diffraction peaks,[26–28] the sample produced by sintering 120 h-milled mixture consists of single $SrFe_{12}O_{19}$ phase, while the sample produced by conventional sinter method consists of $SrFe_{12}O_{19}$ and a small amount of $SrFeO_{2.97}$ in the same sintering conditions (2 h at 1000 °C). The result indicates that the purity is also a influencing factor of the different coercivity of $SrFe_{12}O_{19}$. It is well known that the coercivity of $SrFe_{12}O_{19}$ origin from magneto-crystalline anisotropy, and the Sr ion alternate O ion in the structure of $SrFe_{12}O_{19}$, which result in enhancement of magneto-crystalline anisotropy and improvement of the coercivity. Due to the relative excess of Sr atom, it will inevitably lead to an increase content of Sr ion in the strontium hexaferrite. Obviously, the coercivity of $SrFe_{12}O_{19}$ produced by sintering 120 h-milled mixture is much larger than the other one fabricated by conventional sinter method. However, because of there is a small amount of $SrFeO_{2.97}$ in the $SrFe_{12}O_{19}$ fabricated by conventional sinter method, the pinning of effect of $SrFeO_{2.97}$ is considered carefully.

In the conventional sinter procedures $SrFeO_{2.97}$ reacts with α-Fe_2O_3 to form $SrFe_{12}O_{19}$ finally, while in the sintering 120 h-milled mixture process, the $SrFe_{12}O_{19}$ is obtained by annealing the Sr-containing Fe_3O_4. The intermediate phase is completely different. Besides, the ball milling process is a non-equilibrium process, the ball milling process creates defects which lead to the amorphization of the crystal structure, and improvement of the magnetic properties after annealing is due to the release of stress and the recovery from the defective structure, in agreement with the results of some literature reported previously.[34]

4. CONCLUSION

$SrFe_{12}O_{19}$ was fabricated by two kinds of procedures, respectively:

1. sintering mixture of α-Fe_2O_3 and $SrCO_3$,
2. ball milling of the mixture followed by heat treatment.

The formation mechanism of the $SrFe_{12}O_{19}$ was different in the two kinds of procedures. In the first procedure, the α-Fe_2O_3 reacted with $SrCO_3$ to form an intermediate phase of $SrFeO_{2.97}$ firstly, and then the $SrFeO_{2.97}$ reacted with α-Fe_2O_3 to form $SrFe_{12}O_{19}$ in a sintering temperature ranging from 770 to 960 °C. In the second procedure, the α-Fe_2O_3 reacted with $SrCO_3$ to form Sr-containing Fe_3O_4 with spinel structure when the mixture was milled for 120 h, the $SrFe_{12}O_{19}$ was obtained by annealing the Sr-containing Fe_3O_4 at 700–1000 °C. The saturation magnetization and the coercivity of the $SrFe_{12}O_{19}$ fabricated by the second procedure were 60.65 emu/g and 5481.1 G, respectively. The coercivity of the $SrFe_{12}O_{19}$ fabricated by the second procedure was larger than that of the $SrFe_{12}O_{19}$ produced by the other procedure, which was not related to grain size and phase composition but seems to be the defects in the sample.

Acknowledgments: This work is supported by the Fundamental Research Funds for the Central Universities (Grant No. 2412015KJ007), the Beijing Key Laboratory for Emerging Organic Contaminants Control, the Key Project for Science and Technology Program of Jilin Province (Nos. 20140204028GX and 20150204068GX), the Innovation Science Foundation and Youth Science Foundation of Changchun University of Science and Technology (Grant Nos. XJJLG-2016-07 and XQNJJ-2015-10).

References and Notes

1. M. Anis-ur-Rehman and G. Asghar, *J. Alloys Compd.* 509, 435 (**2011**).
2. M. H. Sousa, F. A. Tourinho, J. Depeyrot, G. J. da Silva, and M. C. F. Lara, *J. Phys. Chem. B* 105, 1168 (**2001**).
3. S. Mekala and J. Ding, *J. Alloys Compd.* 296, 152 (**2000**).
4. S. E. Jacobo, L. Civale, and M. A. Blesa, *J Magn. Magn. Mater.* 260, 37 (**2003**).
5. Y. Lu and W. Song, *Appl. Phys. Lett.* 76, 490 (**2000**).
6. M. N. Ashiq, M. J. Iqbal, and I. H. Gul, *J. Alloys Compd.* 487, 341 (**2009**).
7. G. H. Kim, L. Shao, K. Zhang, and K. P. Pipe, *Nat. Mater.* 12, 719 (**2013**).
8. J. Limpert, F. Stutzki, F. Jansen, T. Eidam, and C. Jauregui, *Light: Sci. Appl.* 1, e8 (**2012**).
9. G. Z. Xing, J. B. Yi, F. Yan, T. Wu, and S. Li, *Appl. Phys. Lett.* 104, 202411 (**2014**).
10. E. M. Dianov, *Light: Sci. Appl.* 1, e12 (**2012**).
11. J. J. Lee, G. Z. Xing, J. B. Yi, T. Chen, M. Ionescu, and S. Li, *Appl. Phys. Lett.* 104, 012405 (**2014**).

12. T. Grossmann, T. Wienhold, U. Bog, T. Beck, and C. Friedmann, *Light: Sci. Appl.* 2, e82 **(2013)**.
13. D. D. Wang, G. Z. Xing, F. Yan, S. Yan, and S. Li, *Appl. Phys. Lett.* 104, 022412 **(2014)**.
14. P. Wang, Y. Wang, and L. Tong, *Light: Sci. Appl.* 2, e102 **(2013)**.
15. D. D. Wang, Q. Chen, G. Z. Xing, J. Yi, and S. R. Bakaul, *Nano Lett.* 12, 3994 **(2012)**.
16. S. V. Sergev, C. Mou, E. G. Turitsyna, A. Rozhin, and S. K.Turitsyn, *Light: Sci. Appl.* 3, e131 **(2014)**.
17. F. Yan, G. Z. Xing, L. Li, and R. M. Wang, *Nature: Scientific Reports* 5, 9128 **(2015)**.
18. J. Guo, J. J. Xie, D. J. Li, G. L.Yang, and F. Chen, *Light: Sci. Appl.* 4, e362 **(2015)**.
19. G. Z. Xing, T. C. Sum, A. Huan, and T. Wu, *Adv. Mater.* 20, 3521 **(2008)**.
20. Z. P. Zhou, B. Yin, and J. Michel, *Light: Sci. Appl.* 4, e35 **(2015)**.
21. G. Z. Xing, J. B. Yi, J. H. Yang, J. Ding, T. C. Sum, and T. Wu, *Appl. Phys. Lett.* 96, 112511 **(2010)**.
22. P. P. Dai, C. Li, and X. T. Zhang, *Light: Sci. Appl.* 5, e16024 **(2016)**.
23. G. Z. Xing, Z. X. Shen, T. C. Sum, and T. Wu, *Phys. Rev. B* 76, 174406 **(2009)**.
24. C. Meng, S. L. Yu, and H. Q. Wang, *Light: Sci. Appl.* 4, e348 **(2015)**.
25. G. Z. Xing, E. J. Sie, A. Sulistio, Q. L. Ye, C. H. A. Huan, T. Wu, and T. C. Sum, *Appl. Phys. Lett.* 98, 102105 **(2011)**.
26. X. C. Li, F. X. Xie, S. Q. Zhang, J. Hou, and W. C. Choy, *Light: Sci. Appl.* 4, e273 **(2015)**.
27. A. Ghasemi, V. Sepelak, X. Liu, and A. Morisako, *J. Appl. Phys.* 107, 09A734 **(2010)**.
28. P. Bercoff, C. Herme, and S. Jacobo, *J Magn. Magn. Mater.* 321, 2245 **(2009)**.
29. H. Wang, Q. He, G. Wen, F. Wang, Z. Ding, and B. Yao, *J. Alloys Compd.* 504, 70 **(2010)**.
30. L. Takacs, *Chem. Soc. Rev.* 42, 7649 **(2013)**.
31. G. Kaupp, *CrystEngComm* 11, 388 **(2009)**.
32. V. Šepelák, A. Düvel, M. Wilkening, K.-D. Becker, and P. Heitjans, *Chem. Soc. Rev.* 42, 7507 **(2013)**.
33. P. Baláž, M. Achimovičová, M. Baláž, P. Billik, Z. Cherkezova-Zheleva, J. M. Criado, F. Delogu, E. Dutková, E. Gaffet, and F. J. Gotor, *Chem. Soc. Rev.* 42, 7571 **(2013)**.
34. G. Mendoza-Suarez, J. Matutes-Aquino, J. Escalante-Garcıa, H. Mancha-Molinar, D. Rıos-Jara, and K. Johal, *J Magn. Magn. Mater.* 223, 55 **(2001)**.

Received: 6 June 2016. Accepted: 23 July 2016.